

Article

# (1E)-1,2-Diaryldiazene Derivatives Containing a Donor- $\pi$ -Acceptor-Type Tolane Skeleton as Smectic Liquid-Crystalline Dyes

Shigeyuki Yamada <sup>1,\*</sup>, Keigo Yoshida <sup>1</sup>, Yuto Eguchi <sup>1</sup>, Mitsuo Hara <sup>2,3</sup>, Motohiro Yasui <sup>1</sup> and Tsutomu Konno <sup>1</sup>

<sup>1</sup> Faculty of Molecular Chemistry and Engineering, Kyoto Institute of Technology, Matsugasaki, Sakyo-ku, Kyoto 606-8585, Japan; m2673040@edu.kit.ac.jp (K.Y.); b0151021@edu.kit.ac.jp (Y.E.); myasui@kit.ac.jp (M.Y.); konno@kit.ac.jp (T.K.)

<sup>2</sup> Department of Molecular and Macromolecular Chemistry, Graduate School of Engineering, Nagoya University, Furo-cho, Chikusa-ku, Nagoya 464-8603, Japan; mhara@chembio.nagoya-u.ac.jp

<sup>3</sup> Faculty of Engineering and Design, Kagawa University, 2217-20, Hayashi-cho, Takamatsu 761-0396, Japan

\* Correspondence: syamada@kit.ac.jp

**Abstract:** Considerable attention has been paid to (1E)-1,2-diaryldiazenes (azo dyes) possessing liquid-crystalline (LC) and optical properties because they can switch color through thermal phase transitions and photoisomerizations. Although multifunctional molecules with both LC and fluorescent properties based on a donor- $\pi$ -acceptor (D- $\pi$ -A)-type tolane skeleton have been developed, functional molecules possessing LC and dye properties have not yet been developed. Therefore, this study proposes to develop LC dyes consisting of (1E)-1,2-diaryldiazenes with a D- $\pi$ -A-type tolane skeleton as the aryl moiety. The (1E)-1,2-diaryldiazene derivatives exhibited a smectic phase, regardless of the flexible-chain structure, whereas the melting temperature was significantly increased by introducing fluoroalkyl moieties into the flexible chain. Evaluation of the optical properties revealed that compounds with decyloxy chains exhibited an orange color, whereas compounds with semifluoroalkoxy chains absorbed at a slightly blue-shifted wavelength, which resulted in a pale orange color. The thermal phase transition caused a slight color change accompanied by a change in the absorption properties, photoisomerization-induced shrinkage, and partial disappearance of the LC domain. These results indicate that (1E)-1,2-diaryldiazenes with a D- $\pi$ -A-type tolane skeleton can function as thermo- or photoresponsive dyes and are applicable to smart windows and in photolithography.

**Keywords:** azo dyes; D- $\pi$ -A-type tolanes; semifluoroalkyl; liquid crystals; thermoresponsiveness; photoresponsiveness



**Citation:** Yamada, S.; Yoshida, K.; Eguchi, Y.; Hara, M.; Yasui, M.; Konno, T. (1E)-1,2-Diaryldiazene Derivatives Containing a Donor- $\pi$ -Acceptor-Type Tolane Skeleton as Smectic Liquid-Crystalline Dyes. *Compounds* **2024**, *4*, 288–300. <https://doi.org/10.3390/compounds4020015>

Academic Editor: Juan C. Mejuto

Received: 13 March 2024

Revised: 5 April 2024

Accepted: 12 April 2024

Published: 17 April 2024



**Copyright:** © 2024 by the authors. Licensee MDPI, Basel, Switzerland. This article is an open access article distributed under the terms and conditions of the Creative Commons Attribution (CC BY) license (<https://creativecommons.org/licenses/by/4.0/>).

## 1. Introduction

Materials whose dye properties change in response to external stimuli, such as heat or electric fields, are called functional dyes and are used in a wide range of applications, such as display devices, energy conversion materials, and recording materials [1–6]. Among the several dyes developed so far, 1,2-diaryldiazenes [7–9], which are well known as azo dyes, primarily exhibit a yellow-to-orange color, and their color changes due to *trans*  $\rightarrow$  *cis* isomerization when irradiated with ultraviolet light. In addition, irradiation with visible light or heating causes *cis*  $\rightarrow$  *trans* isomerization; therefore, 1,2-diaryldiazenes may have potential applications as optical switching materials using reversible photoisomerization [10,11].

Recently, significant attention has been paid to (1E)-1,2-diaryldiazene-based functional molecules that undergo photoisomerization and changes in the aggregate structure in response to temperature, i.e., liquid-crystalline (LC) dyes using a (1E)-1,2-diaryldiazene scaffold as a mesogen. It was reported that polymers with (1E)-1,2-diaryldiazene units introduced into their side chains undergo a phase transition accompanied by photoisomerization from the LC phase to the isotropic (Iso) phase upon light irradiation [12–14].

In addition, LC polymers containing (1*E*)-1,2-diaryldiazene units with one aromatic ring such as the tolane skeleton have been developed, and changes in their birefringence due to photoisomerization were reported [15,16].

Recently, our group explored molecules that have both LC and photoluminescence properties and successfully developed donor- $\pi$ -acceptor (D- $\pi$ -A)-type tolane derivatives that have an electron-donating alkoxy group and an electron-withdrawing cyano group at their molecular ends [17–19]. Among our achievements, the D- $\pi$ -A-type tolane bearing a decyloxy (C<sub>10</sub>H<sub>21</sub>O) chain formed a nematic (N) LC phase as a mesophase (Figure 1a) [19]. However, the formation of a mesophase of smectic A (SmA) was observed when the flexible chain was changed from a decyloxy chain to a semifluoroalkoxy chain, viz., C<sub>4</sub>F<sub>9</sub>-C<sub>6</sub>H<sub>12</sub>O or C<sub>6</sub>F<sub>13</sub>-C<sub>4</sub>H<sub>8</sub>O, in which a fluoroalkyl unit was introduced into the flexible-chain end (Figure 1b) [20]. In addition to their LC properties, these tolanes were found to possess fluorescent properties with a quantum yield ( $\Phi_{PL}$ ) of up to 0.21, even in the crystalline state.

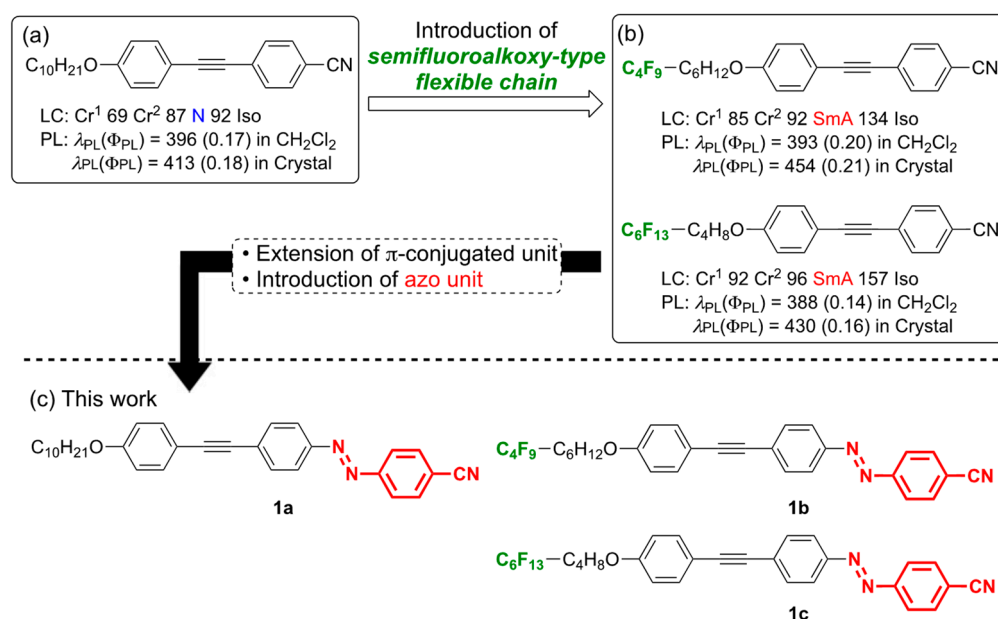


**Figure 1.** Chemical structure of a D- $\pi$ -A tolane containing (a) hydrocarbon chains and (b) semifluoroalkoxy chains developed in previous work. (c) Chemical structures of the target compounds in this work.

Our next focus was on developing LC dyes with LC and dye properties. These are promising functional materials that can produce a wide variety of colors in response to various aggregated structural changes owing to their liquid crystallinity. Because (1*E*)-1,2-diaryldiazene derivatives with a tolane skeleton as a mesogen have hardly been reported, except for the polymer materials mentioned above, we designed D- $\pi$ -A-type tolane derivatives with 4-cyanophenylazo units and various flexible chains introduced at both molecular ends, viz., **1a–c**, (Figure 1c). This paper describes the details of their synthesis and characterization and discusses the effects of the changes in the flexible-chain structure on their properties.

## 2. Materials and Methods

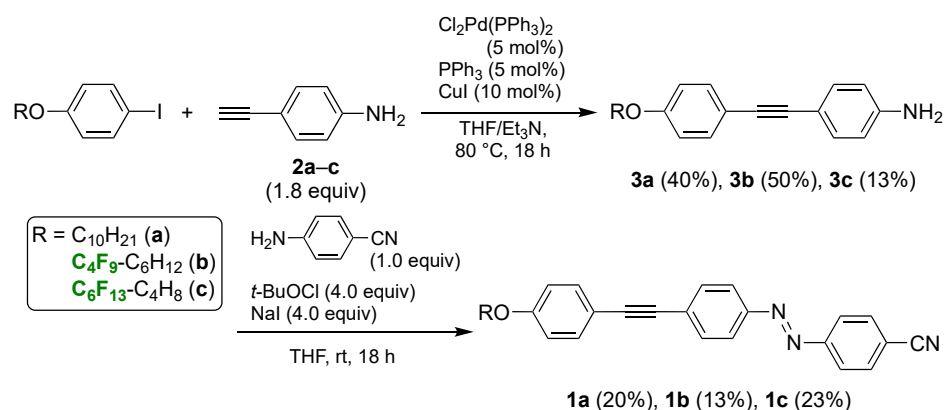
### 2.1. General

<sup>1</sup>H nuclear magnetic resonance (NMR) (400 MHz) and <sup>13</sup>C NMR (100 MHz) spectra were acquired using an AVANCE III 400 NMR spectrometer (Bruker, Rheinstetten, Germany) in chloroform-*d* (CDCl<sub>3</sub>) solution, and chemical shifts are reported in parts per million (ppm) based on the residual protons or carbon in the NMR solvent. <sup>19</sup>F NMR (376 MHz) spectra were acquired using an AVANCE III 400 NMR spectrometer (Bruker, Rheinstetten, Germany) in CDCl<sub>3</sub> solution with C<sub>6</sub>F<sub>6</sub> ( $\delta_F = -163$  ppm) as an internal stan-

dard. Infrared (IR) spectra were recorded using the KBr method on a FTIR-4100 type A spectrometer (JASCO, Tokyo, Japan). All IR spectra are reported in wavenumber ( $\text{cm}^{-1}$ ) units. High-resolution mass spectra (HRMS) were recorded on a JMS700MS spectrometer (JEOL, Tokyo, Japan) using the fast-atom bombardment (FAB) method. Before use, all chemicals of reagent grade were purified using standard methods. The melting temperature ( $T_m$ ) was measured using a DSC-60 differential scanning calorimeter (SHIMADZU, Kyoto, Japan) under a nitrogen atmosphere at a scan rate of  $5\text{ }^\circ\text{C min}^{-1}$ . The reaction progress was monitored by thin-layer chromatography (TLC) using silica gel TLC plates (Merck, Silica Gel, 60F<sub>254</sub>; Rahway, NJ, USA). Column chromatography was performed using silica gel (FUJIFILM Wako Pure Chemical Corporation, Wako-gel<sup>®</sup> 60 N, 38  $\mu\text{m}$  to 100  $\mu\text{m}$ ; Osaka, Japan).

## 2.2. Materials

The (1*E*)-1-(4-cyanophenyl)-2-[4-[2-(4-semifluoroalkoxyphenyl)ethynyl]phenyl]diazenes **1a–c** were synthesized in two steps involving the Pd-catalyzed Sonogashira cross-coupling reaction between 4-(semifluoroalkoxy)-1-iodobenzene and 4-ethynylaniline (**2a–c**), followed by oxidative dimerization with 4-aminobenzonitrile using in situ generated *tert*-butyl hypoiodite (*t*-BuOI) [21,22], according to the reaction sequence shown in Scheme 1. The synthetic procedure for the azo coupling process and the compound characterization data for **1a–c** are as described below. The synthetic details and characterization data for **3a–c** are described in the Supplementary Materials. The <sup>1</sup>H, <sup>13</sup>C, and <sup>19</sup>F NMR spectra of **1a–c** and **3a–c** are shown in Figures S1–S16 in the Supplementary Materials.



**Scheme 1.** Synthetic route to the target compounds **1a–c**.

## 2.3. Typical Synthetic Procedure for

### (1*E*)-1-(4-Cyanophenyl)-2-[4-[2-(4-decyloxyphenyl)ethynyl]phenyl]diazene (**1a**)

A mixture of freshly prepared 4-amino-4'-decyloxytolane (**3a**, 1.15 g, 3.30 mmol), 4-aminobenzonitrile (0.39 g, 3.30 mmol), and NaI (0.96 g, 13.2 mmol) in THF (40 mL) was placed in a 100 mL two-necked round-bottomed flask equipped with a magnetic stirrer bar. *tert*-Butyl hypoiodite (*tert*-BuOCl, 1.56 mL, 13.2 mmol) was added to the solution under an argon atmosphere and stirred at room temperature. After stirring for 18 h, the resultant mixture was poured into an aqueous solution of sodium thiosulfate (Na<sub>2</sub>S<sub>2</sub>O<sub>3</sub>, 50 mL), and the solution was extracted thrice with CH<sub>2</sub>Cl<sub>2</sub> (20 mL). The combined organic extracts were dried over anhydrous sodium sulfate (Na<sub>2</sub>SO<sub>4</sub>) and concentrated under vacuum to provide the crude product, which was purified by silica gel column chromatography using a mixed solution of hexane/CH<sub>2</sub>Cl<sub>2</sub> (*v/v* = 1/1) as the eluent. The title compound was obtained as an orange solid in 20% yield (0.30 g, 0.65 mmol). To evaluate the phase transition and optical properties, the obtained compound was subjected to recrystallization using a 1/1 (*v/v*) mixed solvent system with CHCl<sub>3</sub> as the good solvent and hexane as the poor solvent. Using various spectroscopic techniques, the molecular structure was identified correctly, and purity was proven sufficient for evaluating phase transitions and optical properties.

### 2.3.1. (1E)-1-(4-Cyanophenyl)-2-[4-[2-(4-decyloxyphenyl)ethynyl]phenyl]diazene (1a)

Yield: 20% (orange solid);  $T_m$ : 107 °C on the second heating process;  $^1\text{H NMR}$  ( $\text{CDCl}_3$ ):  $\delta$  0.88 (t,  $J = 6.8$  Hz, 3H), 1.22–1.32 (m, 10H), 1.41–1.50 (m, 2H), 1.79 (quint,  $J = 6.8$  Hz, 4H), 3.98 (t,  $J = 6.8$  Hz, 2H), 6.89 (d,  $J = 8.8$  Hz, 2H), 7.49 (d,  $J = 8.8$  Hz, 2H), 7.66 (d,  $J = 8.8$  Hz, 2H), 7.82 (d,  $J = 8.8$  Hz, 2H), 7.94 (d,  $J = 8.8$  Hz, 2H), 7.99 (d,  $J = 8.8$  Hz, 2H);  $^{13}\text{C NMR}$  ( $\text{CDCl}_3$ ):  $\delta$  14.1, 22.7, 26.0, 26.1, 29.2, 29.3, 29.4, 29.6, 31.9, 68.1, 87.8, 93.3, 114.6, 118.4, 123.38, 123.40, 123.6, 127.9, 129.7, 130.0, 132.3, 133.2, 151.2, 154.5, 159.7; IR (KBr):  $\nu$  3435, 3069, 2956, 2879, 2312, 1577, 1438, 1367, 1070, 957, 790  $\text{cm}^{-1}$ ; HRMS (FAB) Calcd for ( $\text{M}^+$ )  $\text{C}_{31}\text{H}_{33}\text{N}_3\text{O}$ : 463.2624, Found: 463.2629.

### 2.3.2. (1E)-1-(4-Cyanophenyl)-2-[4-[2-(4-(7,7,8,8,9,9,10,10,10-nonafluorodecyloxy)phenyl)ethynyl]phenyl]diazene (1b)

Yield: 13% (orange solid);  $T_m$ : 136 °C on the second heating process;  $^1\text{H NMR}$  ( $\text{CDCl}_3$ ):  $\delta$  1.42–1.60 (m, 4H), 1.66 (quint,  $J = 8.0$  Hz, 2H), 1.83 (quint,  $J = 6.4$  Hz, 2H), 2.00–2.17 (m, 2H), 3.99 (t,  $J = 6.4$  Hz, 2H), 6.88 (d,  $J = 8.8$  Hz, 2H), 7.49 (d,  $J = 8.8$  Hz, 2H), 7.64 (d,  $J = 8.8$  Hz, 2H), 7.66 (d,  $J = 8.8$  Hz, 2H), 7.87 (d,  $J = 8.8$  Hz, 2H), 7.90 (d,  $J = 8.8$  Hz, 2H);  $^{13}\text{C NMR}$  ( $\text{CDCl}_3$ ):  $\delta$  20.1, 25.8, 28.8, 28.9, 30.7 (t,  $J = 22.7$  Hz), 67.8, 87.9, 92.5, 97.8, 114.6, 114.9, 123.1, 124.5, 126.8, 132.2, 133.2, 138.4, 151.4, 152.0, 159.4. The four signals that should be assigned to  $\text{C}_4\text{F}_9$  were split by the F atoms, and their intensities were too low for accurate assignment;  $^{19}\text{F NMR}$  ( $\text{CDCl}_3$ ,  $\text{C}_6\text{F}_6$ ):  $\delta$  -82.34 (t,  $J = 9.4$  Hz, 3F), -115.80 to -116.10 (m, 2F), -125.71 to -125.88 (m, 2F), -127.28 to -127.46 (m, 2F); IR (KBr):  $\nu$  3067, 2938, 2864, 2212, 1592, 1474, 1392, 1287, 1107, 1045, 973, 879  $\text{cm}^{-1}$ ; MS (FAB)  $m/z$  176 ( $[\text{C}_6\text{H}_4\text{-C}\equiv\text{C-C}_6\text{H}_4]^+$ , 100), 130 ( $[\text{N}=\text{N-C}_6\text{H}_4\text{-CN}]^+$ , 6), 104 ( $[\text{C}_6\text{H}_4\text{-N}=\text{N}]^+$ , 21), 102 ( $[\text{PhCN}]^+$ , 20).

### 2.3.3. (1E)-1-(4-Cyanophenyl)-2-[4-[2-(4-(5,5,6,6,7,7,8,8,9,9,10,10,10-tridecafluorodecyloxy)phenyl)ethynyl]phenyl]diazene (1c)

Yield: 23% (orange solid);  $T_m$ : 126 °C on the second heating process;  $^1\text{H NMR}$  ( $\text{CDCl}_3$ ):  $\delta$  1.78–1.97 (m, 4H), 2.09–2.28 (m, 2H), 4.06 (t,  $J = 6.0$  Hz, 2H), 6.95 (d,  $J = 8.8$  Hz, 2H), 7.50 (d,  $J = 8.8$  Hz, 2H), 7.61 (d,  $J = 8.8$  Hz, 2H), 7.67 (d,  $J = 8.8$  Hz, 2H), 7.88 (d,  $J = 8.4$  Hz, 2H), 7.94 (d,  $J = 8.4$  Hz, 2H);  $^{13}\text{C NMR}$  ( $\text{CDCl}_3$ ):  $\delta$  17.3, 28.7, 30.7 (t,  $J = 22.0$  Hz), 67.3, 91.8, 98.0, 114.1, 123.0, 124.5, 130.0, 130.7, 131.3, 133.7, 138.40, 138.41, 145.6, 151.8, 151.9, 159.4. The six signals that should be assigned to  $\text{C}_6\text{F}_{13}$  were split by the F atoms, and their intensities were too low for accurate assignment;  $^{19}\text{F NMR}$  ( $\text{CDCl}_3$ ):  $\delta$  -82.07 (t,  $J = 9.4$  Hz, 3F), -115.66 to -115.94 (m, 2F), -123.14 to -123.40 (m, 2F), -124.10 to 124.34 (m, 2F), -124.80 to -124.98 (m, 2F), -127.37 to -127.54 (m, 2F); IR (KBr):  $\nu$  3631, 3092, 2959, 2846, 2203, 1590, 1512, 1249, 1182, 1042, 980, 856  $\text{cm}^{-1}$ ; MS (FAB)  $m/z$  176 ( $[\text{C}_6\text{H}_4\text{-C}\equiv\text{C-C}_6\text{H}_4]^+$ ,  $[\text{C}_6\text{H}_{12}\text{O-C}_6\text{H}_4]^+$ , 100), 130 ( $[\text{N}=\text{N-C}_6\text{H}_4\text{-CN}]^+$ , 4), 104 ( $[\text{C}_6\text{H}_4\text{-N}=\text{N}]^+$ , 12), 102 ( $[\text{PhCN}]^+$ , 11).

## 2.4. Phase Transition Properties

The phase transition properties were evaluated by polarizing optical microscopy (POM) using a BX53 microscope (Olympus, Tokyo, Japan) equipped with heating and cooling stages (10.002 L, Linkam Scientific Instruments, Redhill, UK). The phase sequences, transition temperatures, and transition enthalpies were determined using differential scanning calorimetry (DSC, Shimadzu DSC-60 Plus) at a heating and cooling rate of 5 °C  $\text{min}^{-1}$  under a  $\text{N}_2$  atmosphere. Variable-temperature powder X-ray diffraction (VT-PXRD) measurements were performed using an FR-E X-ray diffractometer equipped with a two-dimensional R-axis IV detector (Rigaku, Tokyo, Japan) and a  $\text{Cu K}\alpha$  radiation source ( $\lambda = 0.154$  nm).

## 2.5. Photophysical Properties

Ultraviolet–visible (UV–vis) light absorption spectroscopy was performed using a V-750 absorption spectrometer (JASCO, Tokyo, Japan). The transmission method was used to measure the solution samples, and the samples were prepared by dissolving the compounds in  $\text{CH}_2\text{Cl}_2$  and adjusting their concentration to  $1.0 \times 10^{-5}$  mol  $\text{L}^{-1}$ . The diffuse

reflectance method was used to measure the powder samples, and pristine crystalline powders obtained by recrystallization were used.

## 2.6. Theoretical Assessment

Density functional theory (DFT) calculations were performed using the Gaussian 16 (Rev. B.01) suite of programs (Gaussian, Wallingford, CT, USA) [23], and geometry optimizations were performed at the CAM-B3LYP/6-311+G(d,p)//CAM-B3LYP/6-31+G(d) level of theory [24,25] using an implicit solvation model, the conductor-like polarizable continuum model [26], for CH<sub>2</sub>Cl<sub>2</sub>. The vertical electronic transitions were calculated using time-dependent DFT (TD-DFT) at the same level of theory.

## 3. Results and Discussion

Using (1*E*)-1-(4-cyanophenyl)-2-[4-[2-(4-decyloxyphenyl)ethynyl]phenyl]diazene (**1a**), (1*E*)-1-(4-cyanophenyl)-2-[4-[2-(4-(7,7,8,8,9,9,10,10,10-nonafluorodecyloxy)phenyl)ethynyl]phenyl]diazene (**1b**), and (1*E*)-1-(4-cyanophenyl)-2-[4-[2-(4-(5,5,6,6,7,7,8,8,9,9,10,10,10-tridecafluorodecyloxy)phenyl)ethynyl]phenyl]diazene (**1c**) prepared according to Scheme 1, we initially assessed their phase transition properties by DSC and POM. Figure 2 shows the DSC thermograms obtained during the second heating and cooling processes of **1a–c** and the POM textures of **1a–c** in the mesophase (Figures S17–S19). Table 1 summarizes the thermophysical data, including the phase sequences, phase transition temperatures, and phase transition enthalpies of **1a–c**. The detailed phase sequence and transition enthalpies are collected in Tables S1–S3.

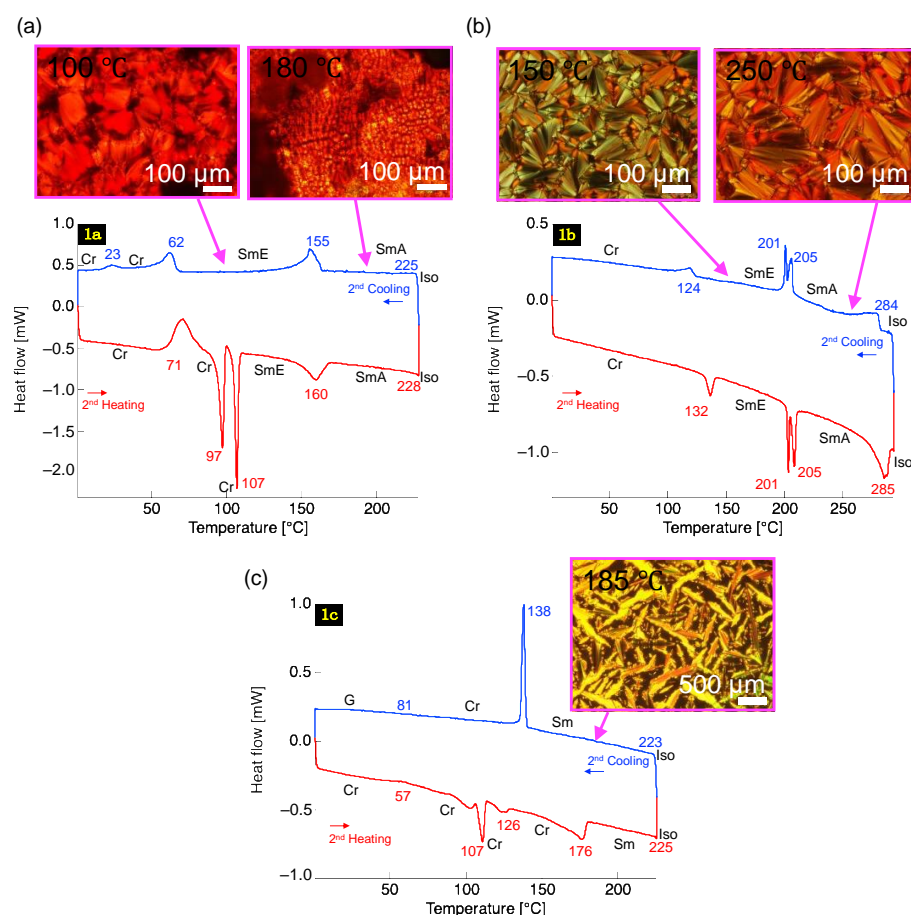


**Figure 2.** DSC thermograms of (a) **1a**, (b) **1b**, and (c) **1c** during the second heating and cooling processes. The values shown in the thermograms indicate the phase transition temperatures. Abbreviations: Cr: crystalline; SmE: smectic E; SmA: smectic A; Sm: unidentified smectic; and Iso: isotropic phases. Inset: POM image in the mesophase.

**Table 1.** Thermophysical data of **1a–c**<sup>1</sup>.

Compound	Phase Sequence and Phase Transition Temperature [°C] (Enthalpy [kJ mol <sup>-1</sup> ])	
<b>1a</b>	[H] [C]	Cr 71 (−9.5) Cr 97 (9.1) Cr 107 (8.1) SmE 160 (4.9) SmA 228 (−) <sup>2</sup> Iso Cr 23 (−0.64) Cr 62 (−4.2) SmE 155 (−6.2) SmA 225 (−) <sup>2</sup> Iso
<b>1b</b>	[H] [C]	Cr 132 (2.2) SmE 205 (6.6) SmA 285 (7.2) Iso Cr 124 (−1.9) SmE 201 (−5.3) SmA 284 (−5.0) Iso
<b>1c</b>	[H] [C]	Cr 57 (−2.2) Cr 107 (8.6) Cr 126 (1.6) Cr 176 (10.9) Sm 225 (−) <sup>2</sup> Iso G 81 Cr 138 (−10.3) Sm 223 (−) <sup>2</sup> Iso

<sup>1</sup> Determined by DSC under a N<sub>2</sub> atmosphere (scan rate: 5.0 °C min<sup>-1</sup>). [H] and [C] represent the second heating and cooling processes, respectively. Abbreviations: Cr, crystalline; SmE, smectic E; SmA, smectic A; Sm, unidentified smectic; Iso, isotropic; G, glassy phase. <sup>2</sup> Determined by POM because the endothermic and exothermic peaks of DSC could not be observed because of thermal decomposition.

Compound **1a**, with a decyloxy chain, was found to form a mesophase during heating and cooling; **1a** is an enantiotropic LC molecule. During the heating process, endothermic peaks of **1a** appeared at 107 °C and 160 °C, which revealed two different mesophases based on POM observation. Upon further heating, the POM image changed to a dark-field texture at 228 °C, indicating a phase transition to an Iso phase. However, at 228 °C, **1a** also decomposed, and no clear endothermic peak was detected by DSC. POM observation revealed that, during the cooling process, a bright-field optical texture appeared at 225 °C, indicating a phase transition to the mesophase. The fact that the POM texture changed to a different form after the exothermic peak at 155 °C suggests that a mesophase-to-mesophase transition occurred. After further cooling, it was found that loss of fluidity occurred owing to energy release at 62 °C, resulting in a phase transition from the mesophase to the crystalline (Cr) phase. During cooling, the POM texture observed in the mesophase in the high-temperature region was a focal-conic fan-shaped texture with small domains, whereas a fan-shaped texture with large domains was observed in the mesophase in the low-temperature region. The POM image observed in the mesophase was a typical texture image of the smectic (Sm) phase, having orientational and positional order; the mesophase formed in **1a** was considered an Sm phase. Compound **1b**, having a short fluoroalkyl moiety at the flexible-chain end, also formed a mesophase exhibiting a fluid bright-field POM texture during both heating and cooling processes and exhibited enantiotropic LC properties. In the POM image of the mesophase, a fan-shaped texture was observed, similar to that of **1a**, and it was concluded that the formed mesophase was the Sm phase (Figure 2b). Compound **1c**, having a longer fluoroalkyl moiety at its flexible-chain end, also exhibited enantiotropic LC properties (Figure 2c). Unlike the other two compounds (**1a** and **1b**), a single mesophase appeared during heating and cooling. The mesophase that appeared could be estimated to be any Sm phase, based on the focal-conic fan-shaped texture observed in the POM image.

The VT-PXRD measurements of **1a** revealed that a diffraction peak corresponding to the (*hkl*) = (001) plane appeared at  $2\theta = 2.17^\circ$  in the high-temperature region (180 °C) during the cooling process (Figures 3a and S20, Tables 2 and S4).

Using Bragg's equation, the interlayer distance (*d*-spacing) corresponding to the diffraction angle was determined as 4.07 nm. Considering that the molecular length calculated by DFT is 3.26 nm, it is presumed to be an SmA phase with a dimer in an antiparallel arrangement as a mesogen [27]. In the low-temperature region (100 °C), diffraction peaks corresponding to the (001) and (002) planes at  $2\theta = 2.34^\circ$  (*d* = 3.77 nm) and  $4.68^\circ$  (*d* = 1.89 nm), respectively, and diffraction peaks corresponding to the (110), (200), and (210) planes in a range of 20–30° were observed. The wide-angle diffraction pattern was a typical SmE phase diffraction pattern; therefore, it can be concluded that the mesophase observed at 100 °C was the SmE. The interlayer distance of the SmE phase formed at 100 °C was 3.77 nm, i.e., smaller than that of the SmA phase formed at 180 °C. This is because, in the SmE phase, the cyanophenyl moiety at the molecular end deeply overlaps with the

alkoxy chain at the other end, causing dense packing [27]. The VT-PXRD measurements of compound **1b** revealed that diffraction peaks corresponding to the (001) and (002) planes were observed at  $2\theta = 2.22^\circ$  ( $d = 3.97 \text{ \AA}$ ) and  $4.38^\circ$  ( $d = 2.01 \text{ \AA}$ ), respectively, in the high-temperature region ( $250 \text{ }^\circ\text{C}$ ) (Figure 3b). Because the molecular length of **1b** is  $3.31 \text{ nm}$  according to DFT calculations, it was determined to be an SmA phase that formed a dimer in an antiparallel arrangement. In the low-temperature region ( $150 \text{ }^\circ\text{C}$ ), in addition to the diffraction peaks at  $2\theta = 2.18^\circ$  ( $d = 4.05 \text{ nm}$ ) and  $4.42^\circ$  ( $d = 2.00 \text{ nm}$ ), diffraction peaks at  $20.14^\circ$  ( $d = 0.44 \text{ nm}$ ),  $22.00^\circ$  ( $d = 0.40 \text{ nm}$ ), and  $27.83^\circ$  ( $d = 0.32 \text{ nm}$ ) were observed. The diffraction peaks that appeared in the wide-angle region corresponded to the surface index ( $hkl$ ) = (110), (200), and (210) diffractions, respectively, and the mesophase formed by these diffractions was concluded to be the SmE phase. When the VT-PXRD measurements were used to determine the mesophase of compound **1c**, thermal decomposition of **1c** occurred along with a phase transition to the Iso phase; therefore, no XRD pattern could be observed in the mesophase.

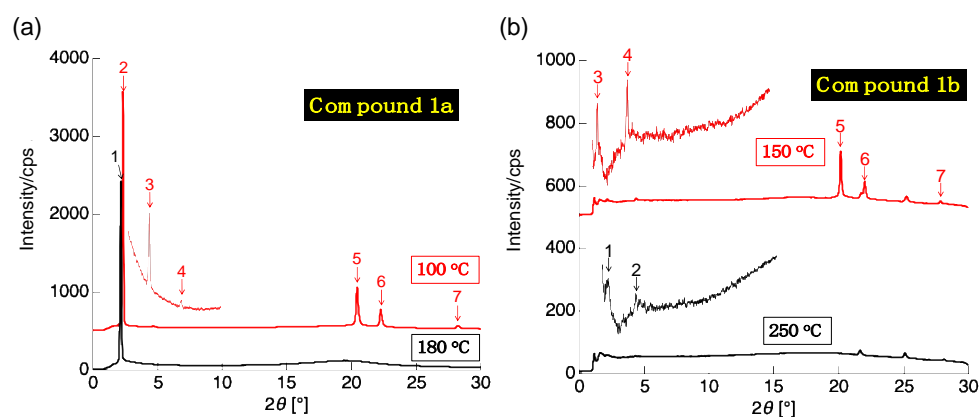


**Figure 3.** VT-PXRD patterns of (a) compound **1a** ( $100 \text{ }^\circ\text{C}$  and  $180 \text{ }^\circ\text{C}$ ) and (b) compound **1b** ( $150 \text{ }^\circ\text{C}$  and  $250 \text{ }^\circ\text{C}$ ).

**Table 2.** PXRD data of **1a**, measured at  $180 \text{ }^\circ\text{C}$  and  $100 \text{ }^\circ\text{C}$ , and **1b**, measured at  $250 \text{ }^\circ\text{C}$  and  $150 \text{ }^\circ\text{C}$ <sup>1</sup>.

1a			1b		
Label	$2\theta$ [ $^\circ$ ]/ $d$ Spacing [nm]	$hkl$	Label	$2\theta$ [ $^\circ$ ]/ $d$ Spacing [nm]	$hkl$
( $180 \text{ }^\circ\text{C}$ )			( $250 \text{ }^\circ\text{C}$ )		
1	2.17/4.07	001	1	2.22/3.97	001
( $100 \text{ }^\circ\text{C}$ )			2	4.38/2.01	002
2	2.34/3.77	001	( $150 \text{ }^\circ\text{C}$ )		
3	4.68/1.89	002	3	2.18/4.05	001
4	7.04/1.25	003	4	4.42/2.00	002
5	20.44/0.43	110	5	20.14/0.44	110
6	22.28/0.40	200	6	22.00/0.40	200
7	28.23/0.32	210	7	27.83/0.32	210

<sup>1</sup> During the cooling process.

Changes in the flexible chains of **1a–c** affected the melting temperature ( $T_m$ ), defined as the phase transition temperature from the Cr phase to the mesophase ( $T_m = 107 \text{ }^\circ\text{C}$  for **1a**,  $132 \text{ }^\circ\text{C}$  for **1b**, and  $176 \text{ }^\circ\text{C}$  for **1c**). Comparing the  $T_m$  of **1a–c**, the alteration from a hydrocarbon-based flexible chain to a semifluoroalkoxy-based flexible chain (**1a** vs. **1b** and **1c**) resulted in a significant increase in  $T_m$  because the fluoroalkyl moiety of the flexible chain stabilized the Cr phase. Additionally, the length of the fluoroalkyl segment also affected the  $T_m$ . As the number of fluoroalkyl segments increased (**1b** vs. **1c**), the aggregation effects between the fluoroalkyl moieties, such as fluorophilic interactions,

became stronger and stabilized the Cr state, resulting in a significant increase in the  $T_m$  of **1c**.

Next, we investigated the dye properties, that is, the UV–vis light absorption properties of **1a–c**. Dilute-solution samples were prepared by dissolving **1a–c** in  $\text{CH}_2\text{Cl}_2$  and adjusting the concentration to  $1.0 \times 10^{-5} \text{ mol L}^{-1}$ . Pristine samples obtained via recrystallization from  $\text{CH}_2\text{Cl}_2/\text{MeOH}$  were used as solid samples. Figure 4 shows the absorption spectra obtained from the UV–vis absorption spectrometry measurements of **1a–c** in dilute solution and solid state (Figure S21), and the theoretical electronic transitions and related molecular orbitals, namely, the highest occupied molecular orbital (HOMO–1), the next highest occupied molecular orbital (HOMO), the lowest unoccupied molecular orbital (LUMO), and the next lowest unoccupied molecular orbital (LUMO+1), calculated by TD-DFT using the molecular structure of **1a** as a representative (Figures S24–S26 for other compounds). The obtained optical data and the calculation results are summarized in Tables 3 and S5–S8.

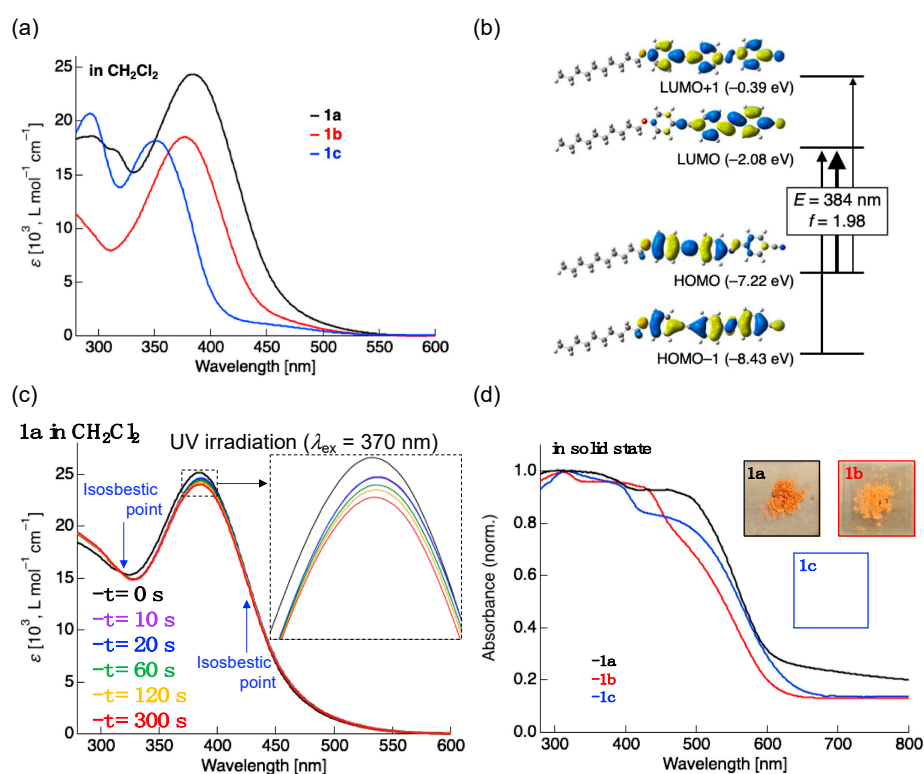


**Figure 4.** (a) UV–vis absorption spectra of **1a–c** in  $\text{CH}_2\text{Cl}_2$  solution (concentration:  $1.0 \times 10^{-5} \text{ mol L}^{-1}$ ). (b) Theoretical electronic transition of **1a** calculated by TD-DFT. (c) UV–vis absorption spectral changes upon UV irradiation ( $\lambda_{\text{ex}} = 370 \text{ nm}$ ). (d) UV–vis diffuse reflection spectra of **1a–c** in the pristine solid state.

A  $\text{CH}_2\text{Cl}_2$  solution of **1a** bearing a decyloxy group as a flexible chain provided an absorption band with a maximum absorption wavelength ( $\lambda_{\text{abs}}$ ) of approximately 384 nm and an absorption band with a  $\lambda_{\text{abs}}$  of approximately 294 nm (Figure 4a). Compound **1b** having a nonafluorodecyloxy group as a semifluoroalkoxy-type flexible chain had a  $\lambda_{\text{abs}}$  of approximately 377 nm, whereas compound **1c** with a tridecafluorodecyloxy group showed two absorption bands with  $\lambda_{\text{abs}}$  of approximately 351 nm and 293 nm. To gain further information about the electronic transitions observed in **1a–c**, we performed TD-DFT calculations at the CAM-B3LYP/6-311+G(d,p)//CAM-B3LYP/6-31+G(d) level of theory [22–25]. The theoretical absorption wavelengths ( $\lambda_{\text{calcd}}$ ) with a large oscillator strength ( $f$ ) were calculated to be 384 nm for **1a** and **1b** and 383 nm for **1c**. Each allowed transition included three interorbital transitions; HOMO  $\rightarrow$  LUMO (78%) was calculated as the primary electronic transition, in addition to HOMO–1  $\rightarrow$  LUMO (14%) and HOMO  $\rightarrow$  LUMO+1 (4%) (Figure 4b). Focusing on the orbital diagrams of the HOMO and LUMO, thought to con-

tribute the most to electronic transitions, it was found that the HOMO lobe was localized in the tolane skeleton, and the LUMO lobe locally covered the azobenzene unit. These results obtained theoretically showed that the absorption band in the long-wavelength region was primarily an intramolecular charge transfer (ICT) transition accompanied by the HOMO  $\rightarrow$  LUMO transition. The energy gap between HOMO and LUMO ( $\Delta E^{H-L}$ ) was 5.13 eV for **1a**, 5.14 eV for **1b**, and 5.16 eV for **1c**, the order of which agreed with that of  $\lambda_{\text{abs}}$ , which was **1a** (384 nm) > **1b** (377 nm) > **1c** (351 nm). Further investigation of the UV–vis absorption spectral changes upon UV irradiation ( $\lambda_{\text{ex}} = 370$  nm) revealed a decrease in the molar absorption coefficient ( $\epsilon$ ) of the absorption band assigned to the ICT  $\pi$ - $\pi^*$  transition ( $\lambda_{\text{abs}} = 384$  nm) after the isosbestic point at 318 nm (Figure 4c for **1a** and Figure S22 for **1b** and **1c**). On the other hand, the  $\epsilon$  of the absorption band assigned to the  $n$ - $\pi^*$  transition of the 1,2-diaryldiazene compounds slightly increased after the isosbestic point at 430 nm (Figure S22). These results strongly suggest the photoisomerization of the 1,2-diaryldiazene compounds from the *trans*- to the *cis*-isomer upon UV irradiation [9,28,29].

**Table 3.** Optical data of **1a–c** measured in  $\text{CH}_2\text{Cl}_2$  solution and theoretical electronic transitions.

Compound	$\lambda$ [nm] <sup>1</sup> ( $\epsilon$ [ $10^3$ , L mol <sup>-1</sup> cm <sup>-1</sup> ])	$\lambda_{\text{calcd}}$ [nm] <sup>2</sup> (Oscillator Strength)	HOMO/LUMO [eV] <sup>2</sup> ( $\Delta E^{H-L}$ )	Theoretical Transition <sup>2</sup> (Contribution)
<b>1a</b>	294 (18.6), 384 (24.3)	384 ( $f = 1.98$ )	-7.22 eV / -2.08 eV (5.13 eV)	HOMO $\rightarrow$ LUMO (78%) HOMO-1 $\rightarrow$ LUMO (14%) HOMO $\rightarrow$ LUMO+1 (4%)
<b>1b</b>	377 (18.5)	384 ( $f = 1.98$ )	-7.23 eV / -2.09 eV (5.14 eV)	HOMO $\rightarrow$ LUMO (78%) HOMO-1 $\rightarrow$ LUMO (14%) HOMO $\rightarrow$ LUMO+1 (4%)
<b>1c</b>	293 (20.7), 351 (18.2)	383 ( $f = 1.98$ )	-7.25 eV / -2.09 eV (5.16 eV)	HOMO $\rightarrow$ LUMO (79%) HOMO-1 $\rightarrow$ LUMO (14%) HOMO $\rightarrow$ LUMO+1 (4%)

<sup>1</sup> In  $\text{CH}_2\text{Cl}_2$  solution (concentration:  $1.0 \times 10^{-5}$  mol L<sup>-1</sup>). <sup>2</sup> Calculated at the CAM-B3LYP/6-311+G(d,p)//CAM-B3LYP/6-31+G(d) level of theory.

The absorption properties of **1a–c** in the pristine solid state were evaluated by diffuse reflection. In the UV–vis diffuse reflection spectrum of **1a**, two broad absorption bands centered at approximately 346 nm and 465 nm were observed, and the color of the pristine solid of **1a** was orange (Figure 4d). Conversely, **1b** and **1c** with semifluoroalkoxy-type flexible chains had absorption spectra that were slightly blue-shifted compared to **1a**, along with a decrease in the absorption intensity on the longer-wavelength side. As a result of the spectral change, the colors of the pristine solids of **1b** and **1c** were also pale orange. The spectral change of **1a–c** in the pristine solid state is attributable to the alteration in the aggregated structures (Figure S20). Compared to the absorption spectra in the  $\text{CH}_2\text{Cl}_2$  solution, which acted as a molecular dispersion system, the absorption spectra of **1a–c** were observed to shift to longer-wavelength regions; all **1a–c** were inferred to form J-aggregate-like structures in the pristine solid state [30,31] owing to the high thermodynamic stabilization caused by the long flexible chains or long fluoroalkyl segments.

Generally, the color of a substance is expected to change due to the phase transition from the Cr to the LC phase because the LC phase has different aggregated structures compared to the pristine solid state. Therefore, we were interested in the absorption properties of compounds **1a–c** in the mesophase after the thermal phase transition (Figures 5 and S21). The measurement sample was prepared by heating the pristine solid to induce a phase transition to the mesophase and then freezing the aggregated structure by dipping it in liquid nitrogen.

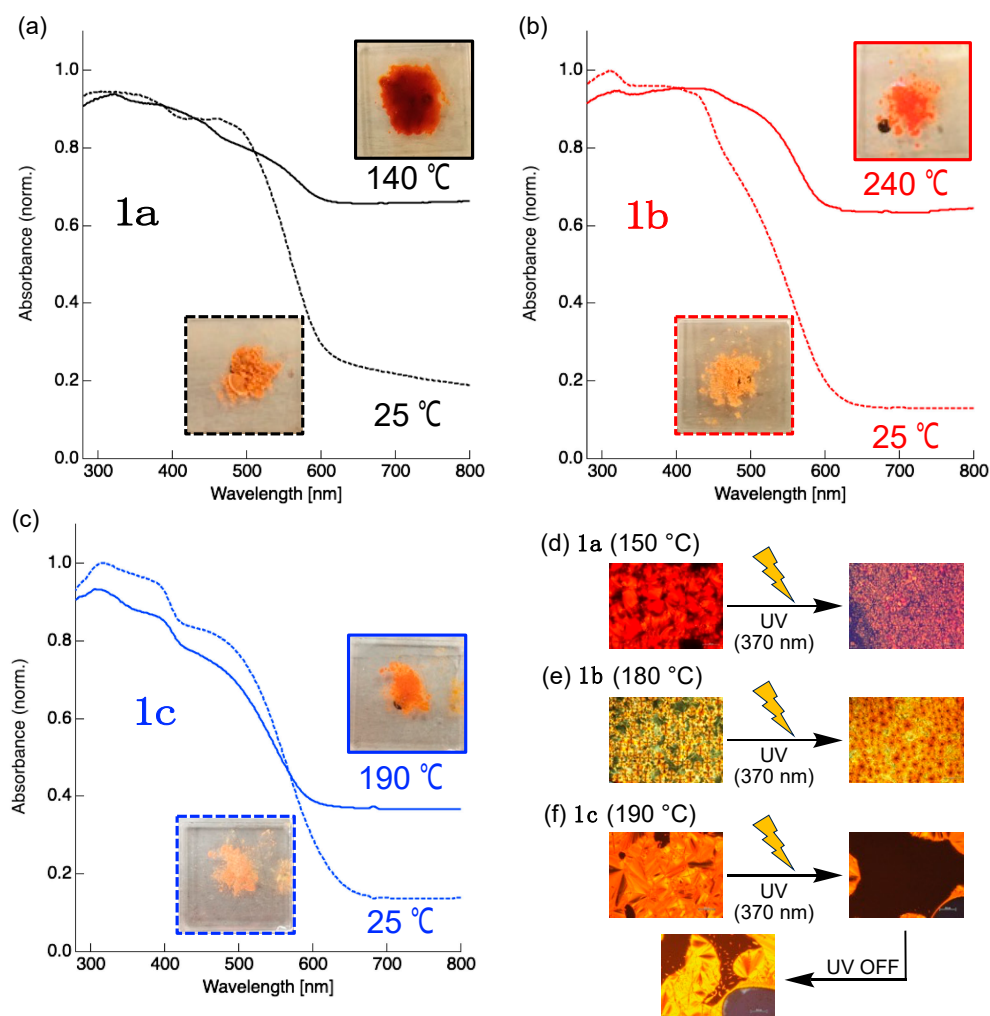


**Figure 5.** UV-vis diffuse reflection spectra of (a) **1a**, (b) **1b**, and (c) **1c** in the pristine solid state and aggregated states of (d) **1a**, (e) **1b**, and (f) **1c** in the mesophase quenched by liquid N<sub>2</sub>.

When the absorption spectra were measured by the diffuse reflection method using the measurement samples prepared as described above, it was found that the absorption intensity on the long-wavelength side increased, whereas the absorption intensity on the short-wavelength side was maintained (Figure 5a–c). The color changed to deep red or deep orange after the thermal phase transition. Furthermore, we were interested in the changes in the mesophase due to photoisomerization (Figure 5d–f). To confirm the photoisomerization behavior in the mesophase, each sample was placed on a heating stage in the POM setup to induce a thermal phase transition and subsequently irradiated with UV light ( $\lambda_{\text{ex}} = 370 \text{ nm}$ ) to investigate the changes in the POM texture. All samples had fan-shaped structures with large domains before UV irradiation; however, upon UV irradiation, the LC domains gradually shrank and partially disappeared (Figures 5d–f and S23). Moreover, for **1c**, which changed to the Iso phase through photoisomerization, it was found that the POM texture in the Sm phase reappeared immediately after stopping UV irradiation (Figure 5f). This phenomenon is similar to the photoresponse behavior of polymers with 1,2-diaryldiazene units in the side chains [14,15], and it was demonstrated that the present molecular system also exhibits the photoresponsiveness associated with *trans*  $\rightarrow$  *cis* photoisomerization.

#### 4. Conclusions

The study designed (1*E*)-1,2-diaryldiazenes, consisting of a D- $\pi$ -A-type tolane skeleton and a 4-cyanophenylazo unit, as LC dyes with both LC and dye-like properties and synthesized three types of (1*E*)-1-(4-cyanophenyl)-2-[4-[2-arylethynyl]phenyl]diazene derivatives

bearing decyloxy, nonafluorodecyloxy, and tridecafluorodecyloxy chains. Using readily available 4-decyloxy- or 4-semifluoroalkoxy-substituted phenylacetylene derivatives as a starting substrate, the target compound was successfully synthesized using two reaction protocols: Sonogashira cross-coupling and oxidative azo-coupling reactions. All three compounds used in this study exhibited enantiotropic LC properties and formed mesophases during both the heating and the cooling processes. POM and VT-PXRD measurements revealed that the compounds with a decyloxy or nonafluorodecyloxy chain showed an SmA phase in the high-temperature region and an SmE phase in the low-temperature region. An analog with a tridecafluorodecyloxy chain, which has a longer fluoroalkyl moiety in the flexible unit, also exhibited enantiotropic LC properties, in which the observed mesophase was the Sm phase, although the detailed mesophase structures were not identified due to thermal decomposition. In addition, the introduction of fluoroalkyl segments into the flexible chain led to a significant increase in  $T_m$ , whereas based on the stratified-dipole array theory, increasing the proportion of fluoroalkyl segments within the flexible chains stabilized the Cr phase and resulted in a significant increase in  $T_m$ . Optical property evaluations showed that all compounds exhibited an orange color in dilute solution, and their absorption wavelengths shifted slightly with modulations in the flexible-chain structure; the introduction of a fluoroalkyl moiety into the flexible chain slightly blue-shifted the absorption wavelength. It was also found that derivatives bearing a fluoroalkyl segment in the flexible chain caused a blue shift in the absorption band to the longer-wavelength side, which gave them a pale orange color even in the solid state, compared to the derivative with a decyloxy chain. The phase transition from the Cr phase to the mesophase changed the aggregated structures, resulting in a darker color tone with an increase in the absorption intensity on the long-wavelength side. Furthermore, when the compounds in the mesophase were irradiated with 365 nm UV light, a reduction in or the disappearance of the LC domain of the POM texture was observed, revealing that the compounds used in this study possess photoresponsiveness. The (1*E*)-1-(4-cyanophenyl)-2-[4-[2-arylethynyl]phenyl]diazene derivatives were found to be multifunctional molecules that exhibit thermoresponsiveness and photoresponsiveness and can be applied to smart windows that change color depending on the temperature and in photolithography, which uses changes in the state of materials due to light stimulation.

**Supplementary Materials:** The following supporting information can be downloaded at: <https://www.mdpi.com/article/10.3390/compounds4020015/s1>, Figures S1–S16: NMR spectra of **1a–c**; Figures S17–S19: DSC thermograms of **1a–c** and POM texture images of **1a–c** in the mesophase; Figure S20: PXRD patterns of **1a** and **1b** at various temperatures; Figure S21: UV–vis absorption (in CH<sub>2</sub>Cl<sub>2</sub> solution) and diffuse reflection spectra (in the pristine solid and aggregated states in the SmA phase) of **1a–c** and photographs of the pristine solid and aggregated states in the SmA phase of **1a–c**; Figure S22: UV–vis absorption spectral changes upon UV irradiation of **1b** and **1c**; Figure S23: POM image of the change of the SmA phase due to UV irradiation of **1a–c**; Figures S24–S26: Molecular orbitals diagrams of **1a–c**; Tables S1–S3: Phase transition data of **1a–c**; Table S4: X-ray diffraction data of **1a** and **1b** measured in the mesophase; Table S5: Theoretical electronic transitions of **1a–c** calculated by the TD-DFT method; Tables S6–S8: Cartesian coordinates of the optimized geometries of **1a–c**.

**Author Contributions:** Conceptualization, S.Y. and K.Y.; methodology, S.Y., K.Y. and M.H.; validation, S.Y. and K.Y.; investigation, S.Y., K.Y., Y.E. and M.H.; resources, S.Y., M.Y. and T.K.; data curation, S.Y., K.Y. and M.H.; writing—original draft preparation, S.Y., K.Y., M.Y. and T.K.; writing—review and editing, S.Y., K.Y., Y.E., M.H., M.Y. and T.K.; visualization, S.Y. and K.Y.; supervision, S.Y.; project administration, S.Y. All authors have read and agreed to the published version of the manuscript.

**Funding:** This research received no external funding.

**Data Availability Statement:** The original contributions presented in this study are included in the article/Supplementary Material, further inquiries can be directed to the corresponding author.

**Acknowledgments:** We would like to express our sincere gratitude to Tsuneaki Sakurai (Kyoto Institute of Technology) for his valuable suggestions and cooperation in the measurements.

**Conflicts of Interest:** The authors declare no conflicts of interest.

## References

1. Ji, C.; Lai, L.; Li, P.; Wu, Z.; Cheng, W.; Yin, M. Organic dye assemblies with aggregation-induced photophysical changes and their bio-applications. *Aggregate* **2021**, *2*, e39. [[CrossRef](#)]
2. Sun, N.; Cai, Y.; Cui, T.; Yang, W.; Hu, Y. Organic dye fluorescent fibers for wearable devices. *Opt. Mater.* **2023**, *143*, 114216. [[CrossRef](#)]
3. Arka, G.N.; Prasad, S.B.; Singh, S. Comprehensive study on dye sensitized solar cell in subsystem level to excel performance potential: A review. *Sol. Energy* **2021**, *226*, 192–213. [[CrossRef](#)]
4. Prajapat, K.; Dhonde, M.; Sahu, K.; Bhojane, P.; Murty, V.V.S.; Shirage, P.M. The evolution of organic materials for efficient dye-sensitized solar cells. *J. Photochem. Photobiol. C* **2023**, *55*, 100586. [[CrossRef](#)]
5. Mukhopadhyay, A.; Zhao, H.; Li, B.; Hamel, J.; Yang, Y.; Cao, D.; Natan, A.; Zhu, H. Abundant organic dye as an anolyte for aqueous flow battery with multielectron transfer. *ACS Appl. Energy Mater.* **2018**, *2*, 7425–7437. [[CrossRef](#)]
6. Moustroph, H.; Stollenwerk, M.; Bressau, V. Current developments in optical data storage with organic dyes. *Angew. Chem. Int. Ed.* **2006**, *45*, 2016–2035. [[CrossRef](#)] [[PubMed](#)]
7. Younis, M.; Ahmad, S.; Atiq, A.; Farooq, M.A.; Huang, M. Recent progress in azobenzene-based supramolecular materials and applications. *Chem. Rec.* **2023**, *23*, e202300126. [[CrossRef](#)] [[PubMed](#)]
8. Zhang, B.; Feng, Y.; Fent, W. Azobenzene-based solar thermal fuels: A review. *Nano-Micro Lett.* **2022**, *14*, 138. [[CrossRef](#)]
9. Bandara, H.M.D.; Burdette, S.C. Photoisomerization in different classes of azobenzene. *Chem. Soc. Rev.* **2012**, *41*, 1809–1825. [[CrossRef](#)]
10. Höglspurger, F.; Vos, B.E.; Hofemeier, A.D.; Seyfried, M.D.; Stövesand, B.; Alavizargar, A.; Topp, L.; Heuer, A.; Betz, T.; Ravoo, B.J. Rapid and reversible optical switching of cell membrane area by an amphiphilic azobenzene. *Nat. Commun.* **2023**, *14*, 3760. [[CrossRef](#)]
11. Derkowska-Zielinska, B.; Skowronski, L.; Sypniewska, M.; Chomicki, D.; Smokal, V.; Kharchenko, O.; Naparty, M.; Krupka, O. Functionalized polymers with strong push-pull azo chromophores in side chain for optical application. *Opt. Mater.* **2018**, *85*, 391–398. [[CrossRef](#)]
12. Ikeda, T.; Tsutsumi, O. Optical switching and image storage by means of azobenzene liquid-crystal films. *Science* **1995**, *268*, 1873–1875. [[CrossRef](#)] [[PubMed](#)]
13. Tsutsumi, O.; Shiono, T.; Ikeda, T.; Galli, G. Photochemical phase transition behavior of nematic liquid crystals with azobenzene moieties as both mesogens and photosensitive chromophores. *J. Phys. Chem. B* **1997**, *101*, 1332–1337. [[CrossRef](#)]
14. Tsutsumi, O.; Kitsunai, T.; Kanazawa, A.; Shiono, T.; Ikeda, T. Photochemical phase transition behavior of polymer azobenzene liquid crystals with electron-donating and -accepting substituents at the 4,4'-positions. *Macromolecules* **1998**, *31*, 355–359. [[CrossRef](#)]
15. Okano, K.; Shishido, A.; Ikeda, T. Photochemical phase transition behavior of highly birefringent azotolane liquid-crystalline polymer films: Effects of the position of the tolane group and the donor–acceptor substituent in the mesogen. *Macromolecules* **2006**, *39*, 145–152. [[CrossRef](#)]
16. Okano, K.; Tsutsumi, O.; Shishido, A.; Ikeda, T. Azotolane liquid-crystalline polymers: Huge change in birefringence by photoinduced alignment change. *J. Am. Chem. Soc.* **2006**, *128*, 15368–15369. [[CrossRef](#)] [[PubMed](#)]
17. Yamada, S.; Konno, T. Development of donor- $\pi$ -acceptor-type fluorinated tolanes as compact condensed phase luminophores and applications in photoluminescent liquid-crystalline molecules. *Chem. Rec.* **2023**, *23*, e202300094. [[CrossRef](#)] [[PubMed](#)]
18. Yamada, S.; Yoshida, K.; Hara, M.; Agou, T.; Yasui, T.; Konno, T. Effects of fluorine atoms introduced into flexible chains or mesogenic structures on their liquid-crystalline and photoluminescence characteristics. *J. Mol. Liq.* **2024**, *393*, 123545. [[CrossRef](#)]
19. Yamada, S.; Yoshida, K.; Kataoka, M.; Hara, M.; Konno, T. Donor- $\pi$ -acceptor-type fluorinated tolane containing a semifluoroalkoxy chain as a condensed-phase luminophore. *Molecules* **2023**, *28*, 2764. [[CrossRef](#)]
20. Yamada, S.; Yoshida, K.; Sakurai, T.; Hara, M.; Konno, T. Effect of fluorine atoms in flexible chains on the phase transitions and photophysical behavior of D- $\pi$ -A-type 4-alkoxy-4'-cyanophenylacetylene. *Mol. Syst. Des. Eng.* **2022**, *7*, 720–724. [[CrossRef](#)]
21. Takeda, Y.; Okumura, S.; Minakata, S. Oxidative dimerization of aromatic amines using *t*BuOI: Entry to unsymmetric aromatic azo compounds. *Angew. Chem. Int. Ed.* **2012**, *51*, 7804–7808. [[CrossRef](#)] [[PubMed](#)]
22. Okumura, S.; Lin, C.; Takeda, Y.; Minakata, S. Oxidative dimerization of (hetero)aromatic amines utilizing *t*-BuOI leading to (hetero)aromatic azo compounds: Scope and mechanistic studies. *J. Org. Chem.* **2013**, *78*, 12090–12105. [[CrossRef](#)] [[PubMed](#)]
23. Frisch, M.J.; Trucks, G.W.; Schlegel, H.B.; Scuseria, G.E.; Robb, M.A.; Cheeseman, J.R.; Scalmani, G.; Barone, V.; Petersson, G.A.; Nakatsuji, H.; et al. *Gaussian 16, Revision B.01*; Gaussian, Inc.: Wallingford, CT, USA, 2016.
24. Yanai, T.; Tew, D.P.; Handy, N.C. A new hybrid exchange-correlation functional using the Coulomb-attenuating method (CAM-B3LYP). *Chem. Phys. Lett.* **2004**, *393*, 51–57. [[CrossRef](#)]
25. Li, M.; Reimers, J.R.; Ford, M.J.; Kobayashi, R.; Amos, R.D. Accurate prediction of the properties of materials using the CAM-B3LYP density functional. *J. Comput. Chem.* **2021**, *42*, 1486–1497. [[CrossRef](#)]
26. Li, H.; Jensen, J.H. Improving the efficiency and convergence of geometry optimization with the polarizable continuum model: New energy gradients and molecular surface tessellation. *J. Comput. Chem.* **2004**, *25*, 1449–1462. [[CrossRef](#)] [[PubMed](#)]

27. Yamamura, Y.; Murakoshi, T.; Hishida, M.; Saito, K. Examination of molecular packing in orthogonal smectic liquid crystal phases: A guide for molecular design of functional smectic phases. *Phys. Chem. Chem. Phys.* **2017**, *19*, 25518–25526. [[CrossRef](#)]
28. Merino, E.; Ribagorda, M. Control over molecular motion using the *cis–trans* photoisomerization of the azo group. *Beilstein J. Org. Chem.* **2012**, *8*, 1071–1090. [[CrossRef](#)] [[PubMed](#)]
29. Tiberio, G.; Muccioli, L.; Berardi, R.; Zannoni, C. How does the *trans–cis* photoisomerization of azobenzene take place in organic solvents? *ChemPhysChem* **2010**, *11*, 1018–1028. [[CrossRef](#)] [[PubMed](#)]
30. Hecht, M.; Würthner, F. Supramolecularly engineered *J*-aggregates based on perylene bisimide dyes. *Acc. Chem. Res.* **2021**, *54*, 642–653. [[CrossRef](#)]
31. Würthner, F.; Kaiser, T.E.; Saha-Möller, C.R. *J*-aggregates: From serendipitous discovery to supramolecular engineering of functional dye materials. *Angew. Chem. Int. Ed.* **2011**, *50*, 3376–3410. [[CrossRef](#)]

**Disclaimer/Publisher’s Note:** The statements, opinions and data contained in all publications are solely those of the individual author(s) and contributor(s) and not of MDPI and/or the editor(s). MDPI and/or the editor(s) disclaim responsibility for any injury to people or property resulting from any ideas, methods, instructions or products referred to in the content.